JOURNAL OF MATERIALS SCIENCE 33 (1998) 2365–2369

Fabrication and transport properties of long–length doped $Bi_{1.7}Pb_{0.3}Sr_2Ca_{2-x}M_xCu_3O_y$ conductors (M=B, Nb or Ag)

M. N. KHAN, A. N. KAYANI
Faculty of Engineering Science, Ghulam Ishaq Khan Institute of Engineering Sciences and Technology, Topi, District Swabi, NWFP, Pakistan
E-mail: mnkhan@giki.Solnpk.undp.org

A. UL. HAQ
Dr A.Q. Khan Research Laboratories, Kahuta, PO Box 502, Rawalpindi, Pakistan

Long lengths of Bi-2223 conductors doped with Ag, Nb and B were fabricated. The recrystallization of the glasses during various heat treatments was studied by differential thermal analysis (DTA), differential scanning calorimetry, X-ray diffraction and resistivity measurements. Activation energies and frequency factors for crystallization were determined by non-isothermal DTA, employing different models. It was found that both the peritectic transition and the reaction rate were dependent on the ambient atmosphere. Kinetic studies under different atmospheres revealed that the thermal stability of Bi-2223 was greatly enhanced under an oxygen atmosphere. J_c measurements at 77 K showed an increase on silver addition. Furthermore it was found that the silver addition does not destroy the superconductivity. © *1998 Chapman & Hall*.

1. Introduction

Over the past few years, several synthesizing techniques have been developed so that superconductors with the desired properties can be obtained. These materials have been used to fabricate superconductors for practical applications. Yet two major issues, namely the kinetics and the stability of the phase, seem to complicate the development of single-phase 2223 superconductors. The 2223 phase is stable only in a very narrow temperature range and the kinetics of its formation is so slow that it is almost impossible to obtain a pure 2223 phase [1–4]. We have previously found that the substitution of lead for bismuth was effective in stabilizing the high-T_c (110 K) phase and demonstrated the formation process of such a high-T_c phase [5]. Our systematic study has also clarified the optimum heat treatment conditions at 855 °C for over 20 h from the viewpoint of T_c (zero). We have also found that the Ca_2PbO_4 phase which is formed during heat treatment plays an important role in the formation of the high-T_c (110 K) phase [6, 7]. On the other hand, further doping of another metal into the Bi–Pb–Ca–Sr–Cu–O system has widely been investigated for glass-derived superconductors and also found to be effective in enhancing T_c (zero) in several cases [8, 9]. In this paper, we discuss the results of doped $Bi_{1.7}Pb_{0.3}Sr_2Ca_{2-x}M_xCu_3O_y$ (M = B, Nb or Ag) glasses with ($x = 0.05, 0.5, 2.0$ and 2.5, their kinetic studies and their superconducting and transport properties.

2. Experimental procedure

Doped Bi-2223 superconductors and long-length conducting rods were prepared by the glass precursor method and powder-in-tube method described in our previous paper [7]. X-ray diffraction (XRD) patterns were recorded with Cu Kα radiation in the 2θ range (20–70°), using an automated diffractometer. Differential thermal analysis (DTA) was carried out in various atmospheres at different heating rates using a Perkin–Elmer DSC-7. The kinetics of crystallization of the glass were investigated from non-isothermal DTA using a Perkin–Elmer DTA-7 at a heating rate of 5–20 °C min^{-1}.

Glass samples were annealed in air for various lengths of time at temperatures selected from the DTA results. Crystalline phases formed in the annealed specimens were identified from powder XRD patterns which were recorded at room temperature. The electrical resistance was measured from 77 to 140 K by the standard four-probe configuration with 1.0 μV cm^{-1} used as the criteria for J_c measurements.

3. Results and discussion

The DTA curves in N_2, O_2 and He atmospheres at a heating rate of 10 °C min^{-1}, are shown in Fig. 1. The glass transition temperatures T_g and the crystallization peak maximum temperatures T_p at different scan rates in the nitrogen atmosphere, for doped and undoped samples are listed in Table I. It was found that

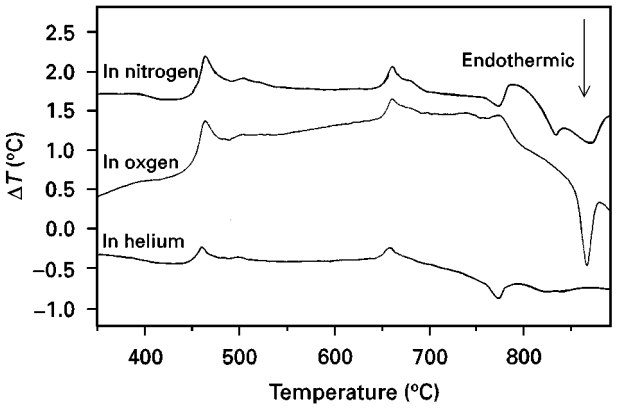

Figure 1 DTA curves in N_2, O_2 and He atmospheres for boron-doped samples at a heating rate of 10 °C min^{-1}.

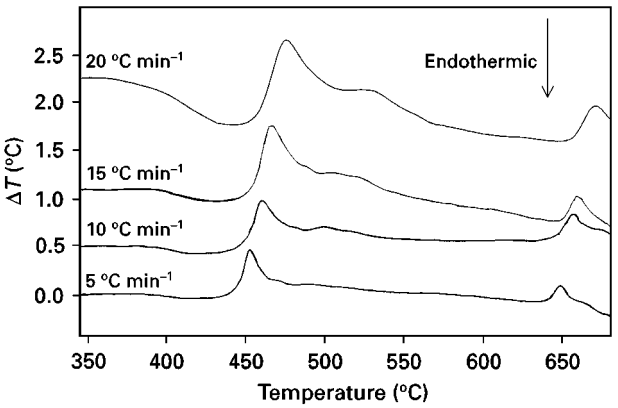

Figure 2 DTA curves in a N_2 atmosphere for boron-doped samples recorded at heating rates of 5–20 °C min^{-1}.

TABLE I T_g and T_p values recorded at different heating rates for $Bi_{1.7}Pb_{0.3}Sr_2Ca_{2-x}B_xCu_3O_y$

Sample	Composition	Heating rate, α (°C min^{-1})	T_g (°C)	T_p (°C)
1	$Bi_{1.7}Pb_{0.3}Sr_2Ca_2Cu_3O_y$	5	401	462
		10	402	471
		15	402	479
		20	404	484
3	$Bi_{1.7}Pb_{0.3}Sr_2Ca_{1.5}B_{0.5}$ Cu_3O_y, first peak	5	398	452
		10	401	460
		15	405	465
		20	406	471
4	$Bi_{1.7}Pb_{0.3}Sr_2Ca_{1.5}B_{0.5}$ Cu_3O_y, second peak	5	398	649
		10	401	656
		15	405	659
		20	406	668

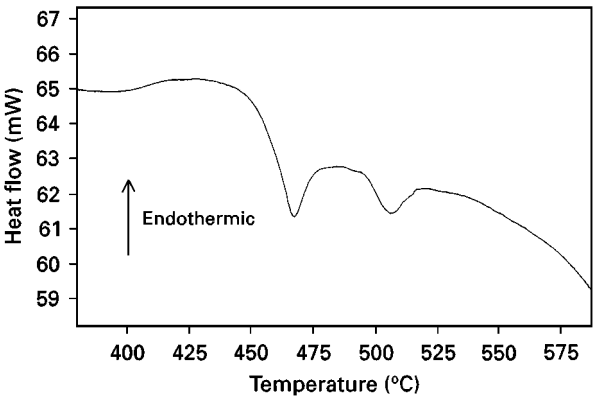

Figure 3 DSC scan for a boron-doped sample in a N_2 atmosphere at a heating rate of 10 °C min^{-1}.

the thermal stability of Bi-2223 samples increased under the oxygen atmosphere as shown in Fig. 1. It was interesting to note from the DTA thermogram of the Nb-doped sample that there were no T_g and T_x peaks, which meant that the sample was already in a crystalline phase.

DTA runs recorded at different heating rates between 5 and 20 °C min^{-1} in a N_2 atmosphere are shown in Fig. 2. A typical differential scanning calorimetry (DSC) scan of a B-doped sample at 10 °C min^{-1} in a N_2 atmosphere is presented in Fig. 3. The endotherm is the glass transition and the exotherm is due to crystallization of the glass.

The peak maximum corresponds to the temperature at which the rate of tranformation of the viscous liquid into crystal becomes maximum. If the number of nucleation sites is increased, e.g., by using slower heating rates, the peak maximum will occur at a temperature at which the melt viscosity is higher, i.e., at a lower temperature. This explains the increase in T_p with increasing scan rate (Table I).

The variable-heating-rate DSC method was employed to evaluate the kinetics of crystallization. The values of kinetic parameters were calculated from the DTA data on Table I and are presented in Table II using the kinetic model of Bansal and Doremus [10]:

$$\ln\left(\frac{T_p^2}{\alpha}\right) = \ln\left(\frac{E}{R}\right) - \ln \nu + \frac{E}{RT_p} \qquad (1)$$

TABLE II Activation energy and Avrami's exponent values for $Bi_{1.7}Pb_{0.3}Sr_2Ca_{2-x}B_xCu_3O_y$

Sample	Composition	Activation energy obtained by Ozawa's (kJ mol^{-1})	Kinetic parameters obtained by the Bansal–Doremus equation			Avrami exponent n
			Activation energy (kJ mol^{-1})	Frequency factor, ν (s^{-1})	K	
1	$Bi_{1.7}Pb_{0.3}Sr_2Ca_2Cu_3O_y$	287.5	275.75	2×10^{17}	0.012	1.62
2	$Bi_{1.7}Pb_{0.3}Sr_2Ca_{1.5}B_{0.5}Cu_3O_y$, first peak	332.7	320.52	48×10^{22}	0.88	1.96
3	$Bi_{1.7}Pb_{0.3}Sr_2Ca_{1.5}B_{0.5}Cu_3O_y$, second peak	525.8	510.33	5.7×10^{26}	0.14	—

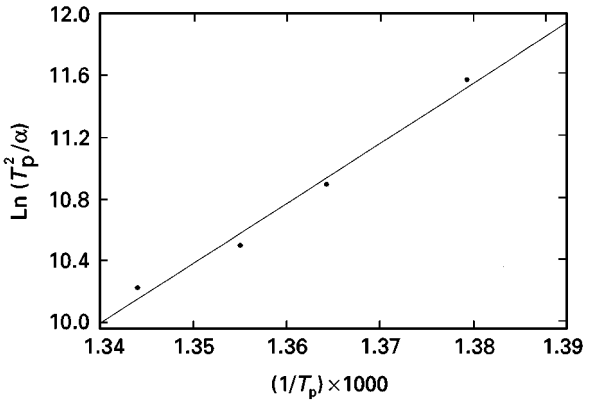

Figure 4 A plot of $\ln(T_p^2/\alpha)$ versus $(1/T_p)$ for the boron-doped sample.

where T_p is the peak maximum temperature, α the heating rate, E the activation energy, R the gas constant and ν the frequency factor. The kinetic parameters, E and ν, are related to the reaction rate constant, K, by the Arrhenius equation

$$K = \nu \exp\left(-\frac{E}{RT}\right) \tag{2}$$

In the derivation of Equation 1 it was assumed that the rate of reaction is a maximum at the peak which is valid assumption for the power-compensated DSC. The plot of T_p^2/α versus $1/T_p$ for the crystallization of the glass was linear, as shown in Fig. 4. From the linear least-squares fitting, values of the kinetic parameters were calculated (Table II). We also calculated the activation energy and the values of Avramis exponent employing Ozawa's technique and Chen's technique as shown in Table II. It is clear from Table II that the values of E for Boron-doped samples compared with undoped samples were greater. Thus it can be concluded that the thermal stability of Bi-2223 doped with boron was greatly increased.

XRD patterns of undoped ($x = 0$) samples annealed at 850 °C for different lengths of time revealed various phases present in the crystallized sample as shown in Fig. 5. Good agreement in both the d values and the intensity ratios of prominent peaks was found with the values reported by Hazen *et al.* [11]. It is evident from the X-ray patterns that the dominant phase is the low-T_c phase. Lattice constants for the low-T_c phase annealed for 25 h are $a = 54.5$ nm, $b = 54.1$ nm and $c = 308.6$ nm. We have also obtained some reflections

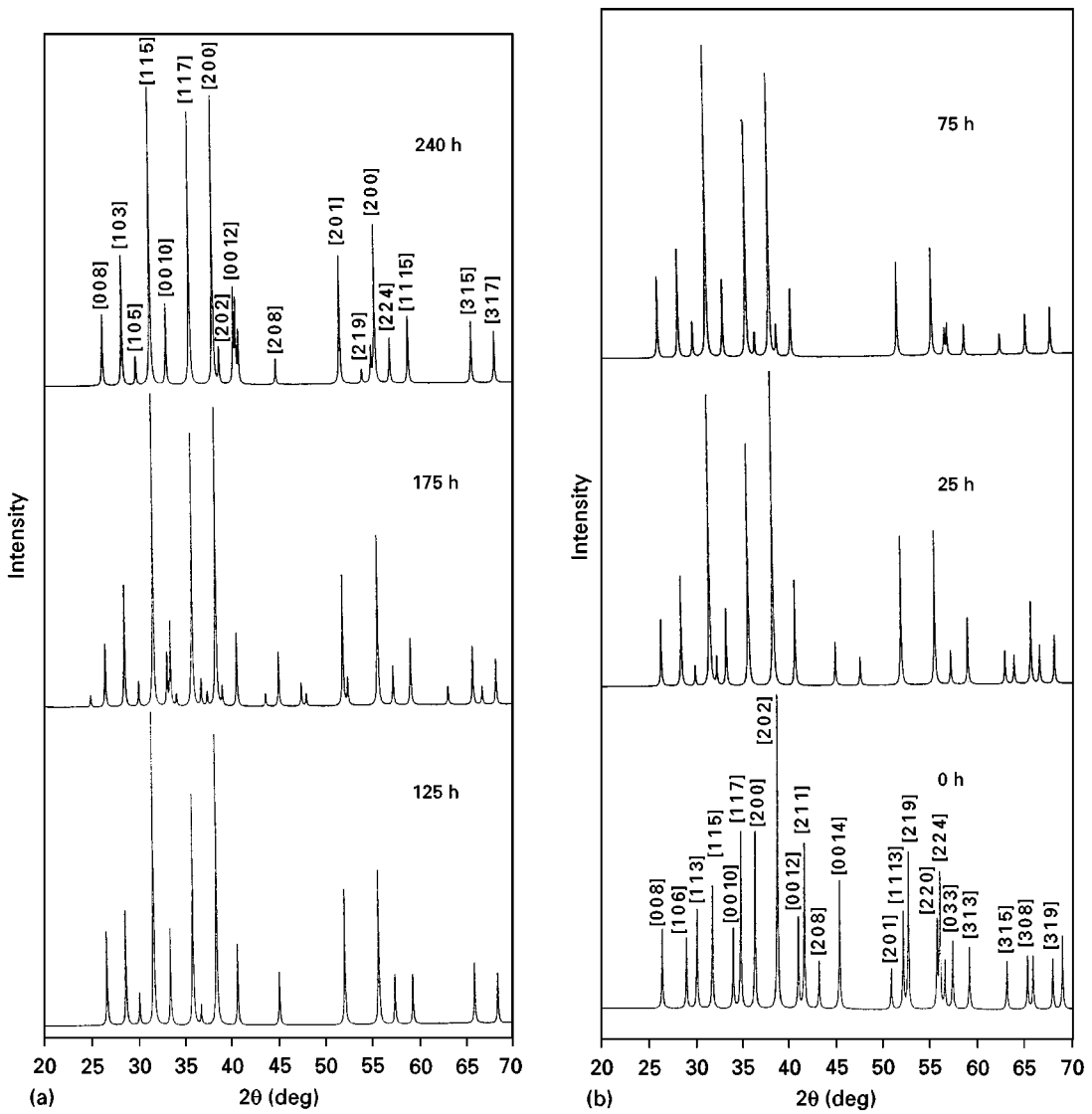

Figure 5 XRD patterns of boron-doped samples annealed at 850 °C for different lengths of time.

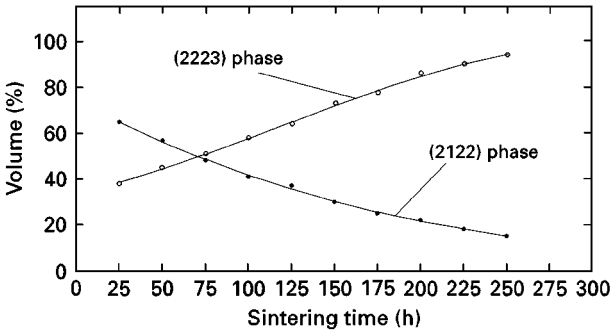

Figure 6 Values of the volume fraction of the high-T_c phase for different sintering times. (○), high-T_c (2223) phase; (●), low-T_c (2122) phase.

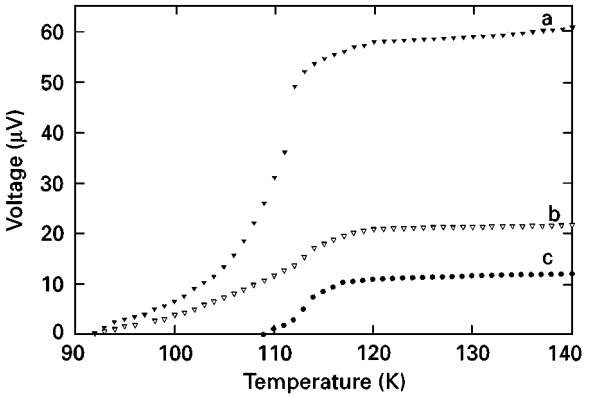

Figure 7 Plot of voltage as a function of temperature for a melt-quenched-and-annealed boron-doped sample (curve a), a sintered boron-doped sample (curve b) and an undoped sample (curve c).

corresponding to the high-T_c (2223) phase and the lattice constants for the sample annealed at 850 °C for 240 h are $a = 56.0$ nm, $b = 52.0$ nm and $c = 377.1$ nm. Similarly, the boron-doped sample annealed for 240 h had the lattice constants $a = 53.9$ nm, $b = 53.8$ nm and $c = 373.6$ nm, and the lattice constants for the same sample annealed for 25 h are $a = 54.3$ nm, $b = 55.1$ nm and $c = 308.2$ nm. This confirmed that the high-T_c (2223) and low-T_c (2212) phases differ mainly in the length of the c-axis. The relative volume fractions of the two phases are calculated by taking into account only the surface characteristics rather than the bulk. We calculated the volume fractions of the low-T_c 2212 and high-T_c 2223 phases as functions of sintering time using the formula

$$\frac{I_H(0\,0\,2)}{I_H(0\,0\,2) + T_L(0\,0\,2)}$$

where $I_H(0\,0\,2)$ and $I_L(0\,0\,2)$ are the peak intensities of the (0 0 2) reflections corresponding to the high-T_c and low-T_c phases. It was found that the volume fraction of the high-T_c (2223) phase increased with increasing sintering time (up to 240 h) while the low-T_c (2212) phase decreased as shown in Fig. 6.

The temperature dependences of the electrical resistance of undoped ($x = 0$) and doped samples are given in Fig. 7. From the comparison with Fig. 6, it becomes obvious that the superconducting properties

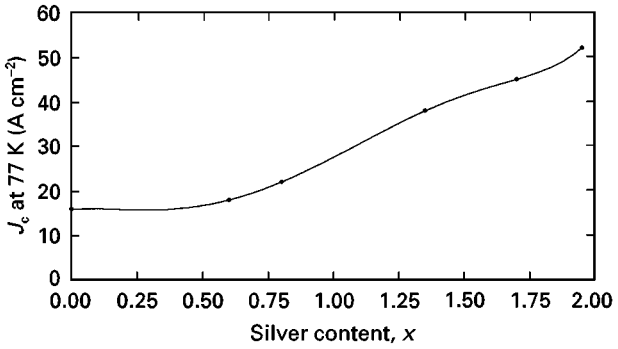

Figure 8 Critical current density, J_c (at 77 K), as a function of silver content in $Bi_{1.7}Pb_{0.3}Sr_2Ca_{2-x}Ag_xCu_3O_y$ at zero field.

such as T_c (zero) are depressed by the dopant species. However, the transition width for the boron-doped sample is greater than for the others. Fig. 8 shows the critical current density at 77 K as a function of silver concentration at zero field. One can see a clear increase in J_c with increasing concentration of silver. The maximum J_c was observed for $x = 3$ and remained constant thereafter. Savvides *et al.* [12] suggested that silver enhances the flux pinning in the intergranular regions, most probably by the development of oxygen point defects at the silver–superconductor interface and at stacking faults around silver grains. Ren *et al.* [13] have confirmed from electron probe microanalysis studies that the silver atoms precipitate at the sites of grain boundaries and cause an interconnection between the grains. These results confirm the migration of metallic silver into the sites of grain boundaries and the creation of superconductor–metal–superconductor regions.

Acknowledgements

We would like to thank the Ghulam Ishaq Khan Institute for providing financial support. The stimulating discussion with and suggestion of boron doping from Dr Ram Kossawsky of Emerging Technologies USA is gratefully acknowledged.

References

1. H. MAEDA, Y. TANAKA, M. FUKUTOMI and T. ASANO, *Jpn. J. Appl. Phys.* **27** (1988) L209.
2. U. BALACHANDRAN, A. N. IYER, P. HALDAR and L. R. MOTOWIDLO, *J. Metals* **45** (1993) 54.
3. D. Y. KAUFMAN, M. T. LANAGAN, S. E. DORRIS, J. T. DAWLEY, I. D. BLOOM, M. C. HASH, N. CHEN, M. R. DEGUIRE, *Appl. Supercond.* **1** (1993) 81.
4. S. X. DOU and H. K. LIU, *J. Supercond. Sci. Technol.* **6** (1993) 297.
5. M. N. KHAN, A. MEMON and S. AL-DALLAL, *Int. J. Mod. Phys. B* **7** (1993) 687.
6. W. ALNASER, M. ZEIN, M. N. KHAN, S. A. DALLAL and A. MEMON, *J. Supercond. Sci. Technol.* **7** (1993) 429.
7. M. N. KHAN and A. UL. HAQ, *J. Mater. Engng Performance* **5** (1996) 445.
8. R. SATO, T. KOMATSU, N. TAMOTO, K. SAWADA, K. MATUSITA and T. YAMASHITA, *Jpn. J. Appl. Phys.* **28** (1989) L1032.
9. M. TATSUMISAGO, S. IJOUE, N. TOHGE and T. MINAMI, *J. Mater. Sci.* **28** (1993) 4193.

10. N. P. BANSAL and R. H. DOREMUS, *J. Therm. Anal.* **29** (1984) 115.
11. R. M. HAZEN, C. T. PREWITH, R. J. ANGEL, N. L. ROSS, L. W. FINGER, C. G. HADIDIACOS and C. W. CHU, *Phys. Rev. Lett*. **60** (1998) 1174.
12. N. SAVVIDES, A. KARSAROS and S. X. DOU, *Physica C* **179** (1991) 361.
13. Y. REN, Z. SENG, J. MENG and P. HE, *Solid State Commun.* **175** (1990) 625.

Received 24 March 1997
and accepted 5 February 1998